Multipole Excitations in Light Neutron-Rich Nuclei

Hiroyuki SAGAWA*) and C. A. BERTULANI *,**)

Center for Mathematical Sciences, The University of Aizu
Aizu-Wakamatsu, Fukushima 965, Japan
**Institute de Fisica, Universidade Federal do Rio de Janeiro*
21945-970, RJ, Brazil

Multipole excitations in neutron-rich light nuclei ^{6}He, ^{11}Li and ^{12}Be with loosely-bound neutrons are studied by using self-consistent Hartree-Fock (H-F) + random phase approximation (RPA) response function theory. The coupling to the continuum is taken into account properly solving the RPA response function in coordinate space. Sharp peaks are found for multipole responses with $J^{\pi} = 0^{+}, 1^{-}$ and 2^{+}, just above the threshold having significant portions of the sum rule strengths. Large extended tails of the loosely-bound neutron wave functions are responsible to cause these low energy strong peaks. The transition densities of the low-energy peaks show quite different radial dependence compared with those of giant resonances.

§1. Introduction

Experimental studies of unstable neutron-rich nuclei have become possible using exotic radioactive beams produced by projectile fragmentation after heavy-ion collisions. The main motivation for these experiments is to determine the masses and the radii of very neutron-rich nuclei which have not been possible to study in the past.[1),2)] Moreover, much attention has been paid recently to study the excitation mode of unstable nuclei.[3)-6)] The light neutron-rich nuclei ^{6}He, ^{11}Li, ^{11}Be and ^{14}Be were observed to have much larger reaction cross sections for medium and high energy heavy-ion collisions[2)] than other neighboring isotopes, and are called "halo" or "skin" nuclei because of the large extension of the wave functions. It has been pointed out[7)-9)] that the loosely-bound nature of neutrons due to the small separation energy and the small orbital angular momentum is responsible to induce the large reaction cross sections of these nuclei, while the intrinsic deformation might be a minor effect.[10)]

It has been discussed theoretically that neutron-rich nuclei might have low-excited dipole resonances caused by the asymmetry of proton and neutron numbers,[11)] and also by the halo neutrons.[7),12)-14)] The former is called "*Pygmy resonances*" and the latter is named "*soft dipole excitations*". Experimental evidence of the soft dipole was reported for ^{11}Li from the analysis of the electromagnetic dissociation cross sections on heavy targets.[3)] Recently, direct measurements of the peaks just above the particle threshold in ^{11}Li and ^{11}Be were achieved by the Coulomb break-up experiment of $^{11}\mathrm{Li} \rightarrow {}^{9}\mathrm{Li} + n + n$[4),5)] and $^{11}\mathrm{Be} \rightarrow {}^{10}\mathrm{Be} + n$.[6)] In this paper, we study multipole excitations not only with $J^{\pi} = 1^{-}$ but also with $J^{\pi} = 0^{+}$

*) E-mail address: sagawa@u-aizu.ac.jp
**) E-mail address: bertu@if.ufrj.br

and 2^+ in nuclei ^{6}He, ^{11}Li and ^{12}Be which have large extension of density profiles due to loosely-bound neutrons.

The self-consistent Hartree-Fock (H-F) and random phase approximation (RPA) response function theory are used to study these excitations.[15),16)] It is shown in Refs. 8) and 17) that the density distributions of neutron-rich nuclei are well described by H-F type wave functions with a constraint for the separation energy. We adopt the H-F wave functions with simple shell model configurations to study both the ground state properties and the excitation modes, taking into account the effect of the separation energy of loosely-bound neutrons properly in the self-consistent model.

Our model has three important advantages to study the excitations of halo nuclei. The first one is that the effect of loosely-bound neutrons on the mean-field potential and at the same time the particle-hole (p-h) interaction is taken into account in a self-consistent way. This self-consistency between the potential and the density will make essential differences between our calculated results and those obtained by the Woods-Saxon or the harmonic oscillator model. Namely, the properties of the responses near the particle threshold reflect unique features of the halo nucleus, as will be discussed later. The second point is the inclusion of the configuration coupling of low excited states to highly excited giant resonances, which was discarded in previous calculations of the cluster-orbital models,[12)] the cluster sum rules,[18)] the shell model Green's function method[19)] and the Faddeev-type three-body model.[20)] In the RPA response function calculation, there is no truncation of the p-h configuration space so that the configuration couplings among the p-h states are fully included. The third point is the continuum effect above the particle threshold which is important to study the width of the excitation spectra. Especially, continuum coupling is essential in neutron drip-line nuclei since it dominates the excitation spectra in low energy region.[21)] We take into account the coupling to the continuum by solving the p-h Green's function in the coordinate space.[16),22)]

As the effective interaction, a parameter set of the density dependent Skyrme force, so called BKN interaction,[23)] is adopted both in the H-F and the RPA calculation. The parameter set of BKN interaction has the effective mass $m^*/m = 1$ and gives realistic single particle energies near the Fermi surface in light nuclei. The original BKN force has no spin-orbit interaction. In our calculations, we introduce the spin-orbit term in the interaction so that the single-particle energy of the last neutron orbit becomes close to the experimental separation energy. In this way, the asymptotic form of the loosely-bound wave function becomes realistic in the neutron-rich nucleus. The p-h interactions of the BKN force are also reasonable as far as the Landau parameters are concerned. In the self-consistent model, the effect of the loosely-bound neutrons is also taken into account on the RPA calculations through the density-dependent p-h interactions.

§2. RPA response function theory

We briefly summarize the RPA response function theory in this section. One can find detailed arguments in the literatures.[15),16)] The RPA Green's function is derived

from the time-dependent H-F (TDHF) theory as a small amplitude approximation:

$$G_{\rm RPA}(\boldsymbol{r_1},\boldsymbol{r_2};E) = G_0(\boldsymbol{r_1},\boldsymbol{r_2};E) + \int G_{\rm RPA}(\boldsymbol{r_1},\boldsymbol{r'};E)V_{\rm ph}(\boldsymbol{r'})G_0(\boldsymbol{r'},\boldsymbol{r_2};E)d\boldsymbol{r'}, \tag{2·1}$$

where G_0 is the unperturbed p-h Green's function, $V_{\rm ph}$ is the residual p-h interaction and E is the excitation energy. The unperturbed response is expressed as

$$G_0(\boldsymbol{r_1},\boldsymbol{r_2};E) = \sum_{\rm p,h}\!\!\!\!\!\!\int \phi_h^*(\boldsymbol{r_1})\phi_p(\boldsymbol{r_1})\left\{\frac{1}{\epsilon_p-\epsilon_h-E+i\eta}+\frac{1}{\epsilon_p-\epsilon_h+E-i\eta}\right\}\phi_p^*(\boldsymbol{r_2})\phi_h(\boldsymbol{r_2}), \tag{2·2}$$

where ϵ_p and ϕ_p (ϵ_h and ϕ_h) are the energy and the wave functions of particle (hole) states. The sum over particle states can be extended also to hole states since the hole-hole contribution from the first term in the bracket is cancelled completely by that from the second term. The sum over all states can be expressed in a closed form,

$$\sum_{i=\rm p,h}\!\!\!\!\!\!\int \phi_i(\boldsymbol{r_1})\frac{1}{\epsilon_i-\epsilon_h\mp(E-i\eta)}\phi_i^*(\boldsymbol{r_2}) = \left\langle \boldsymbol{r_1}\left|\frac{1}{h_0-\epsilon_h\mp(E-i\eta)}\right|\boldsymbol{r_2}\right\rangle, \tag{2·3}$$

where h_0 is the H-F Hamiltonian. When the Skyrme force or the Woods-Saxon potential is used, h_0 is a differential operator and the single-particle Green's function Eq. (3) can be expressed by the product of two linearly independent solutions of the Schrödinger-type equation $(h_0-\epsilon_h\mp E)\psi = 0$. At the origin, ψ is either a regular or irregular solution, while at infinity it is either an exponentially decaying wave or a spherically outgoing wave depending on the value of $\epsilon_h \mp E$.

The transition strength for a one-body operator $\hat{O}_\lambda$ at a given energy E is calculated from the imaginary part of the RPA Green's function $G_{\rm RPA}(E)$,

$$S(E) = \sum_n |\langle n|\hat{O}_\lambda|0\rangle|^2\delta(E-E_n) = \frac{1}{\pi}{\rm Im}\left\{{\rm Tr}[\hat{O}_\lambda^\dagger G_{\rm RPA}(E)\hat{O}_\lambda]\right\}. \tag{2·4}$$

Since $G_{\rm RPA}$ behaves as the product of the transition densities $\delta\rho(\boldsymbol{r_1})\delta\rho(\boldsymbol{r_2})$ in the vicinity of the resonance, the transition density $\delta\rho(\boldsymbol{r_1})$ can be obtained from the RPA response function as well by integrating one of the radial coordinate;

$$\delta\rho(\boldsymbol{r_1}) = \alpha\int G_{\rm RPA}(\boldsymbol{r_1},\boldsymbol{r_2})\hat{O}_\lambda(\boldsymbol{r_2})d\boldsymbol{r_2}, \tag{2·5}$$

where the constant α is determined by the transition strength of the peak.

§3. Results of H-F and RPA calculations

3.1. *H-F results*

We first perform the H-F calculations of nuclei ^{6}He, ^{11}Li and ^{12}Be. The filling approximation is adopted to give the occupation probability of each single-particle orbit. We took the cut-off radius of H-F and RPA calculation to be $R = 30$ fm

Table I. Single particle properties of ^{6}He, ^{11}Li and ^{12}Be. The experimental two neutron separation energies S_{2n} and the calculated single particle energies of the last occupied orbits $\varepsilon_{\rm last}$ are given in the second and third lines in unit of MeV. The r.m.s. mass radii are given in the fourth and fifth lines, while the neutron radii of last orbits are given in sixth and seventh lines in unit of fm. The adopted spin-orbit parameter W_0 is given in the eighth line for each nucleus in units of MeV · fm^5.

	^{6}He	^{11}Li	^{12}Be
S_{2n}(exp)	0.975	0.30	3.67
$\varepsilon_{\rm last}$	0.969	0.263	2.59
$\sqrt{\langle r^2\rangle_m}$ (exp)	2.48±0.03	2.82±0.03	2.82±0.04
$\sqrt{\langle r^2\rangle_m}$ (cal)	2.66	3.08	2.68
$\sqrt{\langle r^2\rangle_{\rm last}}$ (exp)	3.74	5.49	4.21
$\sqrt{\langle r^2\rangle_{\rm last}}$ (cal)	3.67	5.18	3.46
W_0	34	140	175

which is good enough to include properly the loosely bound nature of the neutron wave function. The calculated separation energies of neutrons and r.m.s. radii are tabulated in Table I with experimental data. The radii of last occupied neutron orbits are also given in Table I with corresponding experimental data. The large r.m.s. radii of neutron $1p$ orbits are attributed to the small separation energy. The calculated values are close enough to create the halo structure in the H-F wave functions. In ^{11}Li, the last occupied orbit is taken to be $1p_{1/2}$ orbit although the large mixing of $2s_{1/2}$ configuration is theoretically pointed out recently.[20] The H-F neutron potentials of ^{11}Li and ^{7}Li are shown in Fig. 1. The last neutron $1p_{1/2}$-orbit has a small binding energy 0.263 MeV in ^{11}Li, while all single particle orbits in ^{7}Li

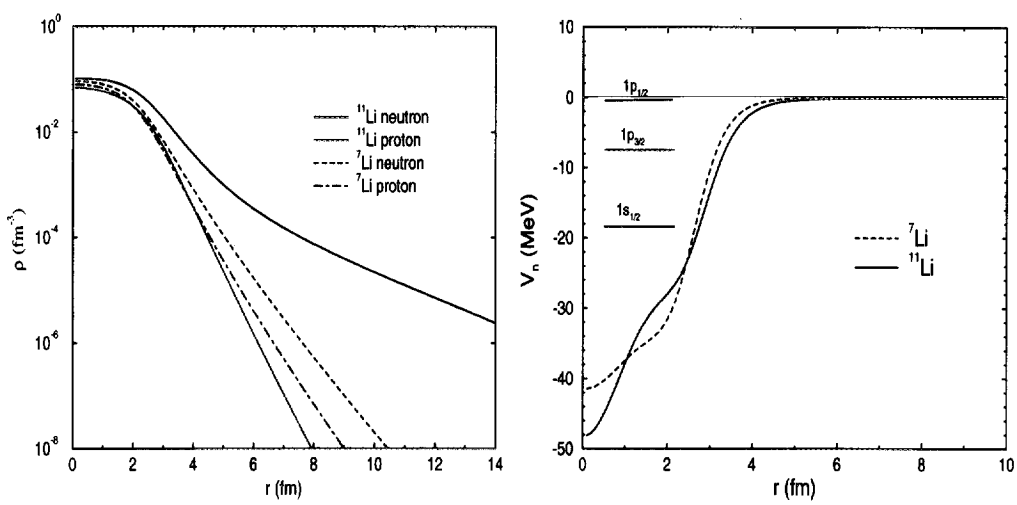

Fig. 1. Neutron H-F potentials and densities in ^{11}Li and ^{7}Li. The Skyrme force BKN interaction is used for the calculations. The spin-orbit strength W_0 for ^{11}Li is given in Table I, while the value W_0=120 MeV · fm^5 is used for ^{7}Li. The calculated neutron single particle energies in ^{11}Li are also shown in the figure.

are well bound in the mean-field potential. The radial dependence of H-F potential of ^{7}Li is similar to that of Woods-Saxon potential. The H-F potential of ^{11}Li shows a different radial dependence from that of ^{7}Li. Namely, there is no clear bottom part of the potential in ^{11}Li and the surface dominates the mean-field. As a result, the potential of ^{11}Li is deeper than that of ^{7}Li in the surface region, while in the region between 1 and 2.5 fm, the potential of ^{7}Li becomes deeper than of ^{11}Li. It is interesting to notice that the same kind of depth difference occurs also between the harmonic oscillator and the Woods-Saxon potentials. This difference is also found in medium heavy nuclei $A \sim 120$ and causes an interesting feature of single particle energies, namely, no $l \cdot l$ dependence of the single particle energies.

The H-F densities of ^{11}Li and ^{7}Li are shown in Fig. 1. It is seen clearly that the neutron density of ^{11}Li has a halo structure compared with other three densities, the neutron density of ^{7}Li and the proton densities of ^{11}Li and ^{7}Li. It is also interesting that the core proton density of ^{11}Li is somewhat different to that of ^{7}Li.

3.2. *RPA for ^{6}He*

There are four peaks in the monopole response of ^{6}He shown at the top of Fig. 2. These peaks are due to the p-h excitations, $(1p_{3/2} \rightarrow 2p_{3/2})_\nu$, $(1p_{3/2} \rightarrow 2p_{3/2})_\pi$, $(1s_{1/2} \rightarrow 2s_{1/2})_\nu$ and $(1p_{3/2} \rightarrow 3p_{3/2})_\nu$ from lower energy to higher energy excitations in order. Due to the threshold effect, there appears a sharp peak at $E_x = 1.6$ MeV, whose main configuration is $(1p_{3/2} \rightarrow 2p_{3/2})_\nu$ excitation. This peak exhausts about 40 % of the energy weighted sum rule (EWSR). In the dipole response, we can see even a broader bump in the energy range $E_x = (0.5 \sim 10)$ MeV, which is due to the neutron excitations from $1p_{3/2} \rightarrow 2s_{1/2}$ and $1p_{3/2} \rightarrow 1d_{5/2}$. The peaks at higher excitation energies, $E_x = 12$ and 19 MeV, are due to proton excitations. Since these p- and sd-shell proton orbits are bound states in the H-F potential, the transition strengths are not seen in the imaginary part of the unperturbed response although the real part has the poles at the corresponding energies. The peaks have the width due to the coupling to the continuum in the RPA response. The dipole transition strengths between $E_x = (0.5 \sim 4)$ MeV have 6.5 % of EWSR, while those between $E_x = (0.5 \sim 10)$ MeV exhaust 19 % of EWSR. The quadrupole response in ^{6}He has also a sharp peak starting from just above the threshold energy. The peak in the energy $E_x = (0.5 \sim 2.6)$ MeV exhausts 12 % of EWSR, while the strengths at higher energy around $E_x = 20$ MeV have a large portion of EWSR.

The transition densities of two peaks at $E_x = 1.4$ MeV and 15.5 MeV in the monopole response are shown in Fig. 3. The peak at $E_x = 15.5$ MeV has a typical radial dependence as the collective monopole state. On the other hand, the peak just above the threshold is dominated by a long tail inherent to the loosely-bound neutron excitation. The transition densities of dipole response are shown in the middle part of Fig. 3. That of the threshold peak has a node at around $r = 2$ fm, while the giant dipole at E_x=19 MeV has a typical Tassie type transition density showing a peak at the nuclear surface. The radial dependences of the quadrupole transition densities show quite similar features to those of the dipole. Namely, that of the giant resonance at E_x=20 MeV has a surface peak, while the threshold peak

has rather long extension of the transition density.

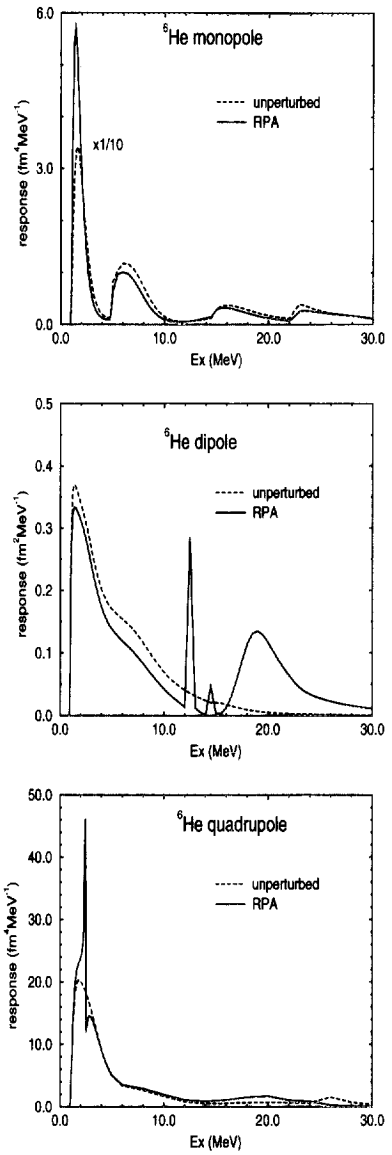

Fig. 2. RPA responses for isoscalar monopole, isovector dipole and isoscalar quadrupole transitions in ^{6}He. The solid curves are RPA responses, while the dashed curves correspond to unperturbed responses.

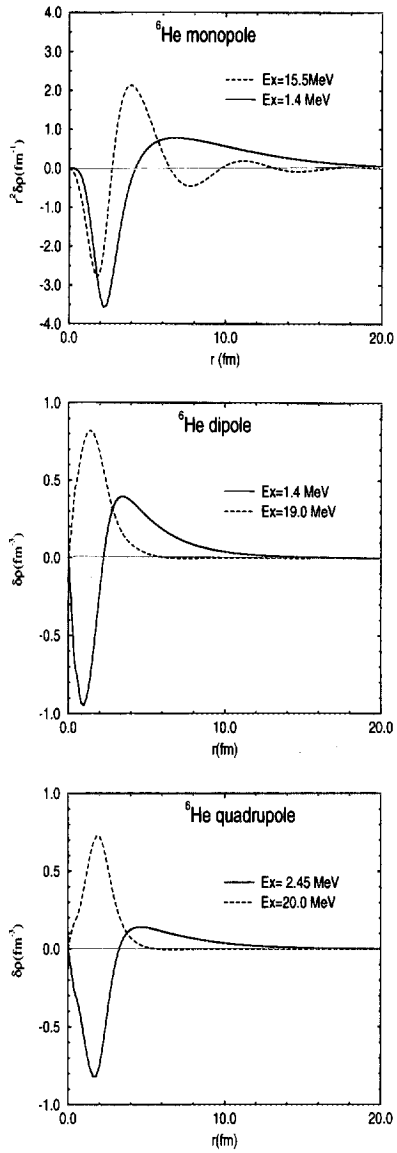

Fig. 3. The transition densities of several peaks in RPA responses of ^{6}He. The energy of each peak is indicated in the figures. The absolute magnitude of the transition density is normalized to reproduce the transition strength of each peak according to Eq. (2·5).

3.3. *RPA for ^{11}Li*

The monopole, dipole and quadrupole responses in ^{11}Li are shown in Fig. 4. For each response, the threshold effect due to the halo neutrons gives a sharp large peak

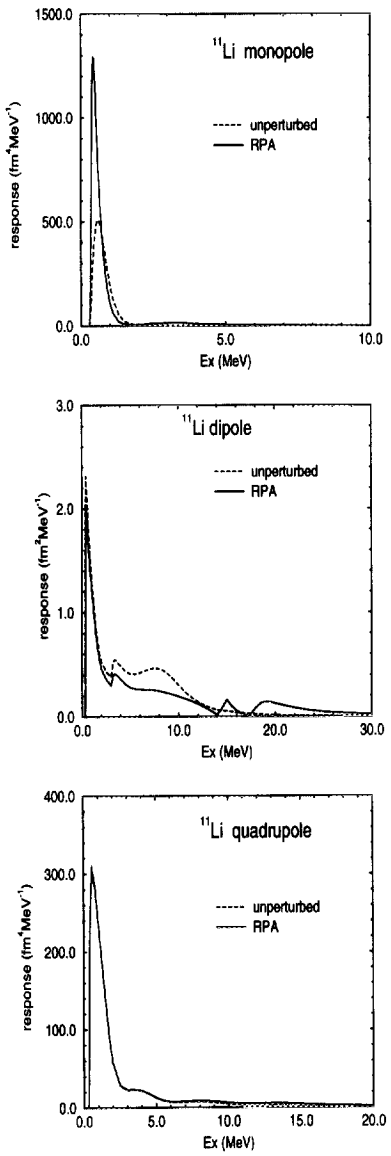

Fig. 4. RPA responses for isoscalar monopole, isovector dipole and isoscalar quadrupole transitions in ^{11}Li. The solid curves are RPA responses, while the dashed curves correspond to unperturbed responses.

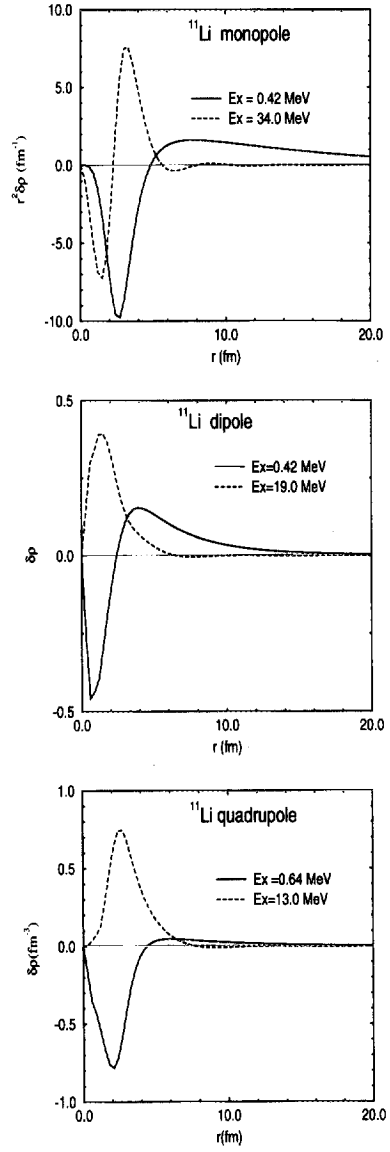

Fig. 5. The transition densities of several peaks in RPA responses of ^{11}Li. The energy of each peak is indicated in the figures. The absolute magnitude of the transition density is normalized to reproduce the transition strength of each peak according to Eq. (2·5).

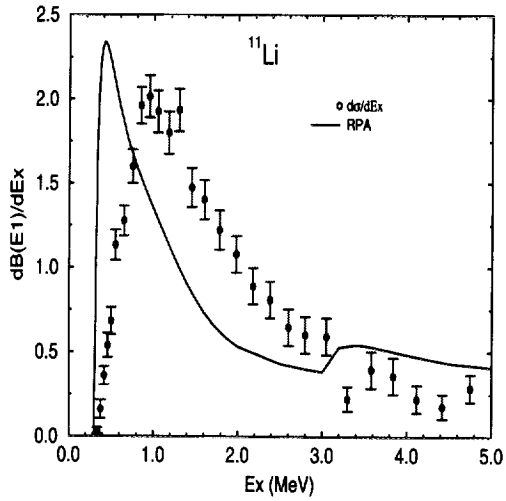

Fig. 6. Dipole strength distributions in ^{11}Li. The solid curve is calculated by the present RPA response theory, while the experimental data denoted by the circles are taken from Ref. 5).

just above the threshold. In the cases of monopole and quadrupole, the threshold peak is the dominant peak exhausting 35 % and 20 % of the monopole and quadrupole EWSR, respectively. The dipole response is also shown in the middle part of Fig. 4. In the dipole case, the response has several peaks at the energy region just above the threshold at $E_x = (3 \sim 10)$ MeV and also at the giant resonance energy region. The first and the second peaks are due to the p-h excitations of halo neutrons $(1p_{1/2} \rightarrow s_{1/2})_\nu$ and $(1p_{1/2} \rightarrow d_{3/2})_\nu$, while those in the giant resonance energy are mainly due to the proton p-h excitations. The peak at the threshold around $E_x = (0.3 \sim 3)$ MeV exhausts 5.0 % of the EWSR.

In Fig. 6, the calculated response is compared with the experimental data which was recently obtained by Riken group.[5] It is remarkable that the calculated strength distribution gives good agreement with the observed data, not only in the energy dependence, but also the absolute magnitude. The difference in the peak energy might be due to the lack of pairing correlations in the present RPA calculation.

The transition densities of strong peaks in the response of ^{11}Li are given in Fig. 5. The main features of these densities are quite similar to those in ^{6}He. Namely, those of the threshold states have a node and a large extended tail outside of the core, while the giant resonances have surface peak transition densities like the Tassie ones.

3.4. *RPA for ^{12}Be*

The RPA response of the three multipoles in ^{12}Be are shown in Fig. 7. The strength distributions are more fragmented in ^{12}Be compared with those of ^{6}He and ^{11}Li. This is partly due to more available p-h configurations, and partly due to weak threshold effect in ^{12}Be. The threshold peaks exhaust 18 % ($E_x = (2.5 \sim 10)$ MeV), 1.4 % ($E_x = (2.5 \sim 4)$ MeV) and 8.6 % ($E_x = (2.5 \sim 8.5)$ MeV) of the EWSR, respectively, for the monopole, the dipole and the quadrupole responses.

The large peaks at higher energies are due to the bound proton p-h excitations, which are not seen in the unperturbed response. The RPA correlations are rather strong in the dipole and the quadrupole responses, and give large bumps at $E_x = 17$ MeV

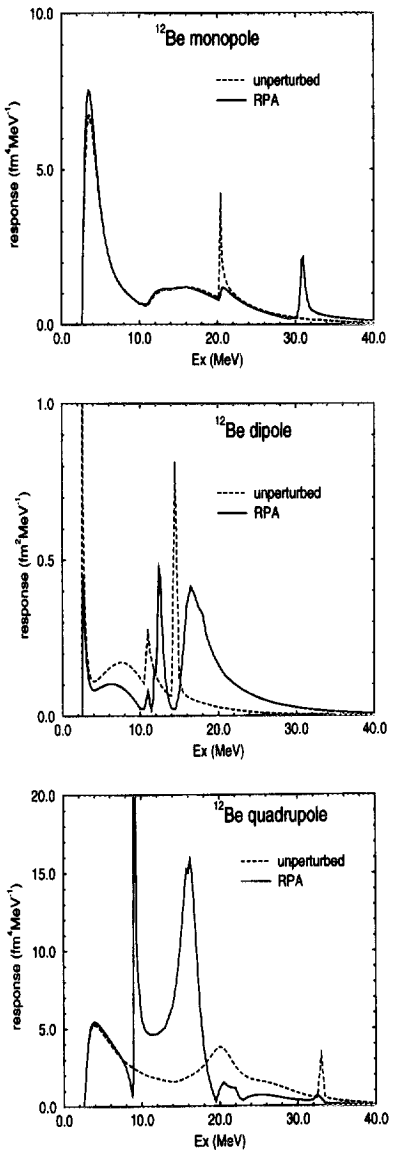

Fig. 7. RPA responses for isoscalar monopole, isovector dipole and isoscalar quadrupole transitions in ^{12}Be. The solid curves are RPA responses, while the dashed curves correspond to unperturbed responses.

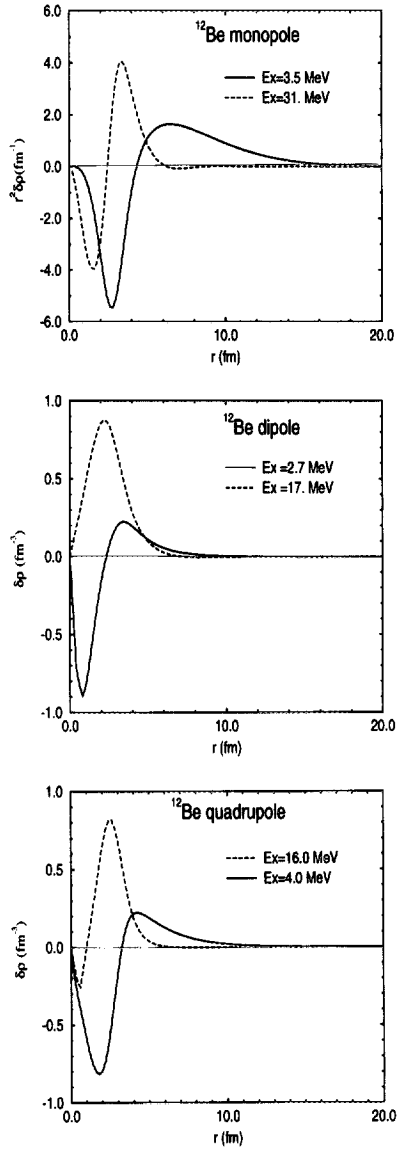

Fig. 8. The transition densities of several peaks in RPA responses of ^{12}Be. The energy of each peak is indicated in the figures. The absolute magnitude of the transition density is normalized to reproduce the transition strength of each peak according to Eq. (2·5).

for the dipole response and at $E_x = (10 \sim 20)$ MeV for the quadrupole response. The transition densities of the threshold peaks and also highly excited states with large transition strengths are shown in Fig. 8. It is interesting that the essential features of these densities are almost the same as those of ^{6}He and ^{11}Li, although the strength distributions are substantially different.

§4. Summary

In summary, we studied the multipole responses with $J^\pi = 0^+, 1^-$ and 2^+ in the neutron dripline nuclei ^{6}He, ^{11}Li and ^{11}Be by using the self-consistent H-F+RPA response function theory. We found strong peaks having significant portions of the sum rule values at $E_x \sim 1$ MeV with the narrow widths for three multipoles $J^\pi = 0^+, 1^-$ and 2^+ in ^{6}He and ^{11}Li. The dominant p-h configurations of these peaks are the excitations of the halo neutrons in the $1p$-orbit. The multipole responses of ^{12}Be have more structure than the other two nuclei because of small halo components in the wave functions. The large transition strengths of these low-excited states are caused by the long-extended tail of halo wave function which might be common in many neutron drip line nuclei. We have shown that the transition densities of the low-lying peaks are quite different from the Tassie-type ones and have much longer tails than that of the ground state. It might be quite interesting to study these peaks experimentally by using direct break-up in heavy ion reactions, inelastic heavy ion reactions with radioactive beams and charge-exchange reactions. The calculated dipole peak just above the threshold is compared with experimental data in ^{11}Li which was obtained recently by the measurement of the direct break-up of ^{11}Li. Two data show reasonable agreement in the energy dependence and also in the absolute magnitude.

Acknowledgments

The author would like to thank M. Ishihara and K. Nakamura for stimulating discussions.

References

1) For example, see, C. Detraz and D. C. Vieira, Ann. Rev. Nucl. Part. Sci. **39** (1989), 407.
I. Tanihata, *Treatise on Heavy-Ion Science* , ed. D. A. Bromley (Plenum Press, New York and London, 1989), vol. 8, p. 443.
E. Roeckl, Rep. Prog. Phys. **55** (1992), 1661.
A. C. Mueller and B. M. Sherrill, Ann. Rev. Nucl. Part. Sci. **43** (1993), 529.
2) I. Tanihata, T. Kobayashi, O. Yamakawa, S. Shimoura, K. Ekuni, K. Sugimoto, N. Takahashi, T. Shimoda and H. Sato, Phys. Lett. **B206** (1988), 592.
3) T. Kobayashi, S. Shimoura, I. Tanihata, K. Katori, K. Matsuta, T. Minamisono, K. Sugimoto, W. Müller, P. L. Olson, T. J. M. Symons and H. Wieman, Phys. Lett. **232B** (1989), 51.
4) K. Ieki et al., Phys. Rev. Lett. **70** (1993), 730.
5) S. Shimoura et al., Phys. Lett. **B348** (1995), 29.
6) T. Nakamura et al., Phys. Lett. **B331** (1994), 296.
7) P. G. Hansen and B. Johnson, Europhys. Lett. **4** (1987), 409.
8) H. Sagawa, Phys. Lett. **B286** (1992), 7.

9) D. V. Fedorov, A. S. Jensen and K. Riisager, Phys. Lett. **B312** (1993), 1.
10) H. Kitagawa, N. Tajima and H. Sagawa, Z. Phys. A, to be published.
11) A. M. Lane, Ann. of Phys. **63** (1971), 171.
B. Gyarmati, A. M. Lane and J. Zimanyi, Phys. Lett. **50B** (1974), 316.
M. Harvey and F. C. Khanna, Nucl. Phys. **A221** (1974), 77.
12) Y. Suzuki and Y. Tosaka, Nucl. Phys. **A517** (1990), 599.
13) T. Hoshino, H. Sagawa and A. Arima, Nucl. Phys. **A523** (1991), 228.
14) G. F. Bertsch and J. Foxwell, Phys. Rev. **C41** (1990), 1300; also see Phys. Rev. **C42** (1990), 1159.
15) G. F. Bertsch and S. F. Tsai, Phys. Rep. **18C** (1975), 126.
K. F. Liu and N. Van Giai, Phys. Lett. **65B** (1976), 23.
16) N. Van Giai and H. Sagawa, Nucl. Phys. **A371** (1981), 1.
17) G. F. Bertsch, B. A. Brown and H. Sagawa, Phys. Rev. **C39** (1989), 1154.
18) H. Sagawa and M. Honma, Phys. Lett. **251B** (1990), 17.
19) H. Esbensen and G. Bertsch, Nucl. Phys. **A542** (1992), 310.
20) M. V. Zhukov et al., Phys. Rep. **231** (1993), 151.
21) H. Hamamoto, H. Sagawa and X. Z. Zhang, Phys. Rev. **C53** (1996), 765.
H. Hamamoto and H. Sagawa, Phys. Rev. **C53** (1996), R1492.
22) S. Shlomo and G. Bertsch, Nucl. Phys. **A243** (1975), 507.
23) P. Bonche, S. Koonin and J. W. Negele, Phys. Rev. **C13** (1976), 1226.